

Bulk photovoltaic effects in altermagnets

Motohiko Ezawa¹

¹Department of Applied Physics, The University of Tokyo, 7-3-1 Hongo, Tokyo 113-8656, Japan

(Dated: March 25, 2025)

The bulk photovoltaic effect is a photocurrent generation from alternating electric field, which is a promising candidate for future efficient solar cell technology. It is the second-order optical current, which is the injection current or the shift current. We focus on the direct current generation. By employing a simple two-band model of the d -wave altermagnet coupled with the Rashba interaction, we show that the linearly polarized light can generate the injection and shift currents when the Néel vector points to an in-plane direction. The magnitude of the injection current is almost constant over a wide range of the frequency ω of the applied light provided it is smaller than a certain critical frequency ω_c and larger than the bulk gap energy ε_{gap} , $\varepsilon_{\text{gap}} < \hbar\omega < \hbar\omega_c$. Hence, the use of the injection current is quite efficient for solar cell technology because any photon whose energy is within this range can be equally utilized.

Introduction: Nonlinear optical responses are fascinating, upon which there are intensive research. When we apply an alternating electric field $E(\omega)$ with the frequency ω , there are two types of the second-order responses. One is the second-harmonic generation proportional to 2ω . The other is a direct current (dc) generation. The latter is important in the context of photovoltaic effects. Recently, bulk photovoltaic effects[1–6] including the injection current[4, 5, 7–9, 11, 13, 14] and the shift current[2–5, 8, 9, 11, 13–20] attract much attention because they provide more efficient photovoltaic effects than the usual one based on the p - n junction for the application to solar cell devices. Indeed, only the photon having the same energy $\hbar\omega$ as the band gap is transformed to a current in the p - n junction. On the other hand, the second-order current is generated for the photon with the energy larger than the band gap, which is the injection current or the shift current. There are several experimental observation of bulk photovoltaic effects[22–26].

Altermagnets constitute one of the most active fields of condensed matter physics[27–29]. It has zero net magnetization as in the case of an ordinary antiferromagnet, but breaks time-reversal symmetry and has a momentum dependent energy spectrum[27–36]. These features open a way to future ultra-high density spintronic memories with ultrafast switching in the order of ps[37] because there is no stray field owing to the zero net magnetization. There are some studies on nonlinear responses as well on the altermagnet[38–40].

In this paper, we study photovoltaic effects in the d -wave altermagnet with the Rashba interaction based on a simple two-band model, where the Néel vector points to an in-plane direction. The dc current generation by the second-order optical process is studied. We summarize the results in Fig.1. The photocurrent generation occurs only when the energy of a photon is within a certain range $\varepsilon_{\text{gap}} < \hbar\omega < \hbar\omega_c$, where ε_{gap} is the bulk gap energy and ω_c is the critical frequency. A photon contributes to the shift current but the efficiency decreases for large energy as $1/\omega$ as in Fig.1(b). On the other hand, a photon contributes almost equally to the injection current as in Fig.1(c). Hence, it would be useful to employ the d -wave altermagnet to generate the injection current for future solar cell technology. Incidentally, in the p - n junction, only a photon whose energy is identical to the bulk gap ε_{gap} contributes to the current ($\hbar\omega = \varepsilon_{\text{gap}}$) as in Fig.1(a).

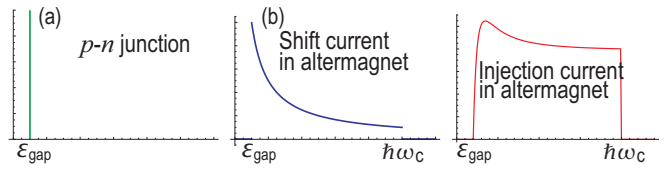


FIG. 1. Illustration of photovoltaic current as a function of the energy $\hbar\omega$ of the photon. (a) In the case of the p - n junction, only a photon with the energy $\hbar\omega = \varepsilon_{\text{gap}}$ contributes to the current. (b) A photon with the energy $\varepsilon_{\text{gap}} < \hbar\omega < \hbar\omega_c$ contributes to the shift current but the efficiency decreases for large energy as $1/\omega$, where $\hbar\omega_c$ is a certain critical photon energy. (c) A photon with the energy $\varepsilon_{\text{gap}} < \hbar\omega < \hbar\omega_c$ contributes almost equally to the injection current. The vertical axis is the magnitude of photovoltaic current, while the horizontal axis is the energy $\hbar\omega$ of the applied photon.

Injection current and shift current: The current density j induced by the applied electric field E is expanded as

$$j^c = \sigma^{c;a} E_a + \sigma^{c;ab} E_a E_b + \dots \quad (1)$$

The first term is the linear response and the second term is the second-order nonlinear response. If we apply an alternating electric field, the second-order response has a form

$$j^c(\omega_1 + \omega_2) = \sigma^{c;ab}(\omega_1 + \omega_2; \omega_1, \omega_2) E_a(\omega_1) E_b(\omega_2). \quad (2)$$

In this paper, we investigate the dc current generation,

$$j^c(0) = \sigma^{c;ab}(0; \omega, -\omega) E_a(\omega) E_b(-\omega). \quad (3)$$

In the following, we use the abbreviation $j^c \equiv j^c(0)$ and $\sigma^{c;ab}(\omega) \equiv \sigma^{c;ab}(0; \omega, -\omega)$.

We apply incident light propagating along the z direction. We consider the linear polarized light,

$$E^\uparrow = E_0(\cos \phi, \sin \phi, 0) \quad (4)$$

with the polarization ϕ , and the circularly polarized light,

$$E^\circlearrowleft = \frac{E_0}{\sqrt{2}}(1, i, 0), \quad E^\circlearrowright = \frac{E_0}{\sqrt{2}}(1, -i, 0). \quad (5)$$

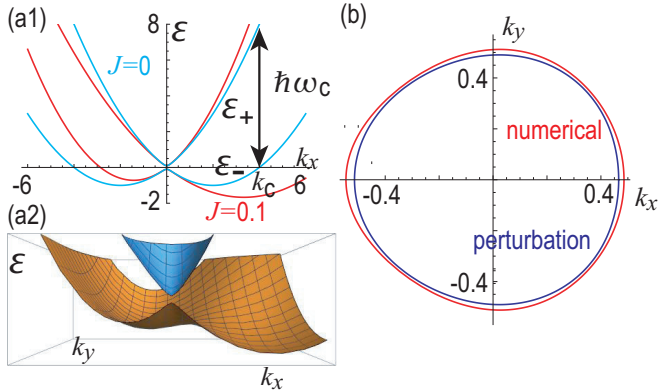


FIG. 2. (a1) Energy spectrum $\varepsilon_{\pm}(\mathbf{k})$. The vertical axis is the energy ε in units of ε_0 . The horizontal axis is k_x in units of k_0 . The red and cyan curves represent the energy spectrum in the case of $J = 0.1\varepsilon_0/k_0^2$ and $J = 0$, respectively. (a2) Bird's eye's view in the case of $J = 0.1\varepsilon_0/k_0^2$. (b) $k(\phi)$ at $\hbar\omega = 0.4\varepsilon_0$ in the case of $J = 0.1\varepsilon_0/k_0^2$. The red ellipse is the Fermi surface of the original model, while the blue ellipse is that of the perturbation theory given in Eq.(16). We have set $B = 0.1\varepsilon_0$.

The conductivities are given by[9, 10]

$$\begin{aligned}\sigma^{c;\uparrow}(\Phi) &= \text{Re}\sigma^{c;xx}\cos^2\Phi + \text{Re}\sigma^{c;yy}\sin^2\Phi \\ &\quad + 2\text{Re}\sigma^{c;xy}\cos\Phi\sin\Phi, \\ \sigma^{c;\odot} &= \text{Re}\sigma^{c;xx} + \text{Re}\sigma^{c;yy} + 2\text{Re}\sigma^{c;xy}, \\ \sigma^{c;\circlearrowleft} &= \text{Re}\sigma^{c;xx} + \text{Re}\sigma^{c;yy} - 2\text{Im}\sigma^{c;xy}.\end{aligned}\quad (6)$$

The injection current is in general given by the formula[4, 5, 7–9, 11–14]

$$\begin{aligned}\sigma_{\text{inject}}^{c;ab} &= -\tau \frac{2\pi e^3}{\hbar^2} \int \frac{d^3k}{(2\pi)^3} \sum_{n,m} (f_n - f_m) \Delta_{mn}^c \\ &\quad \times r_{nm}^b r_{mn}^a \delta(\omega_m - \omega_n - \omega),\end{aligned}\quad (7)$$

where τ is the relaxation time, a is the lattice constant, $f_n = 1/(\exp(\varepsilon_n - \mu) + 1)$ is the Fermi distribution function for the band n , μ is the chemical potential, ε_n is the energy of the band n , $r_{mn}^a = \langle m | i\partial_{k_a} | n \rangle$ is the Berry connection and $\Delta_{mn}^c = v_{mm}^c - v_{nn}^c$ is the interband transition of the velocity $v_{mn}^c = \frac{1}{\hbar} \langle m | i\partial_{k_c} H | n \rangle$. The injection current is nonzero when the velocity of the energy dispersion is imbalanced between the conduction and valence bands along the c direction.

On the other hand, the shift current is in general given by the formula[2–5, 8, 9, 11, 13–20]

$$\begin{aligned}\sigma_{\text{shift}}^{c;ab} &= -\frac{\pi e^3}{\hbar^2} \int \frac{d^3k}{(2\pi)^3} \sum_{n,m} (f_n - f_m) (R_{mn}^{c,a} - R_{nm}^{c,b}) \\ &\quad \times r_{nm}^b r_{mn}^a \delta(\omega_m - \omega_n - \omega),\end{aligned}\quad (8)$$

where $R_{mn}^{c,a} = r_{mm}^c - r_{nn}^c + i\partial_{k_c} \log r_{mn}^a$ is the shift vector[5]. The shift vector is gauge invariant although the Berry connection is not gauge invariant. The shift vector describes the mean position of the Wannier function. The shift current is nonzero

when the mean positions are different between the conduction and valence bands.

It is known[11, 13, 41–47] that the injection (shift) current can be generated by the linearly (circularly) polarized light in magnetic system due to the time-reversal symmetry breaking.

Altermagnet: We consider a two-dimensional system made of the d -wave altermagnets with the Rashba interaction, whose Hamiltonian is given by[27–29]

$$\begin{aligned}H(\mathbf{k}) &= \frac{\hbar^2 (k_x^2 + k_y^2)}{2M} I_2 + \lambda (k_x \sigma_y - k_y \sigma_x) \\ &\quad + J (k_x^2 - k_y^2) \mathbf{n} \cdot \boldsymbol{\sigma} + B \sigma_z,\end{aligned}\quad (9)$$

where M is the effective mass of the free electrons, I_2 is the 2×2 identity matrix, λ is the magnitude of the Rashba interaction, J is the magnitude of the d -wave altermagnetization, and \mathbf{n} is the Néel vector of the d -wave altermagnet. We set $\mathbf{n} = (0, 1, 0)$. The Rashba interaction is introduced by placing an altermagnet on the substrate[27–29, 39, 40, 48–51]. The last term $B\sigma_z$ is introduced by magnetization, or by applying an external magnetic field, or by the Edelstein effect due to the Rashba splitting under in-plane electric field.

The d -wave magnet in two dimensions is realized in organic materials[30], perovskite materials[33], and twisted magnetic Van der Waals bilayers[52]. The d -wave altermagnet in three dimensions is realized in RuO_2 [53–57], Mn_5Si_3 [58] and FeSb_2 [59].

The Hamiltonian (9) preserves inversion symmetry in the absence of the Rashba interaction. The Rashba interaction breaks inversion symmetry, while the altermagnet term breaks time-reversal symmetry. Hence, the system breaks both inversion symmetry and time-reversal symmetry. The inversion symmetry breaking is necessary for the presence of the second-order optical responses. We assume $|J| < \hbar^2/(2M)$ so that the parabolic dispersion is positive for large $k = |\mathbf{k}|$.

Photovoltaic effects: The Hamiltonian (9) is of the form,

$$H = h_0(\mathbf{k}) I_2 + \sum_{j=x,y,z} h_j(\mathbf{k}) \sigma_j,\quad (10)$$

describing a two-band system. The energy spectrum consists of $\varepsilon_{\pm}(\mathbf{k}) = h_0(\mathbf{k}) \pm \varepsilon(\mathbf{k})$ with $\varepsilon(\mathbf{k}) = \sqrt{\sum_{j=x,y,z} h_j^2}$.

The energy spectrum is illustrated in Fig.2(a), where there is a Dirac cone at the Γ point ($k_x = k_y = 0$) with the bulk band gap $\varepsilon_{\text{gap}} = 2|B|$. We set the chemical potential zero ($\mu = 0$). We now examine the condition imposed on the frequency ω for the photocurrent generation to occur. The optical transition occurs from the occupied valence band ($f_- = 1$) to the unoccupied conduction band ($f_+ = 0$) at the energy $\varepsilon_+ - \varepsilon_- = 2\varepsilon = \hbar\omega$. Thus, we may set $f_- - f_+ = 1$ in the injection current (7) and the shift current (8). Furthermore, by examining the energy spectrum in Fig.2(a), the optical transition is found to occur only when the frequency ω of a photon is within the range $\varepsilon_{\text{gap}} < \hbar\omega < \hbar\omega_c$, where the critical frequency ω_c is determined as $\hbar\omega_c = 2\varepsilon(\mathbf{k}_c)$ with the use of \mathbf{k}_c which is the solution of $\varepsilon_-(\mathbf{k}_c) = 0$ for the conduction band.

We study the injection and shift currents under the linearly and circularly polarized light. We may set $m = +$ and $n = -$

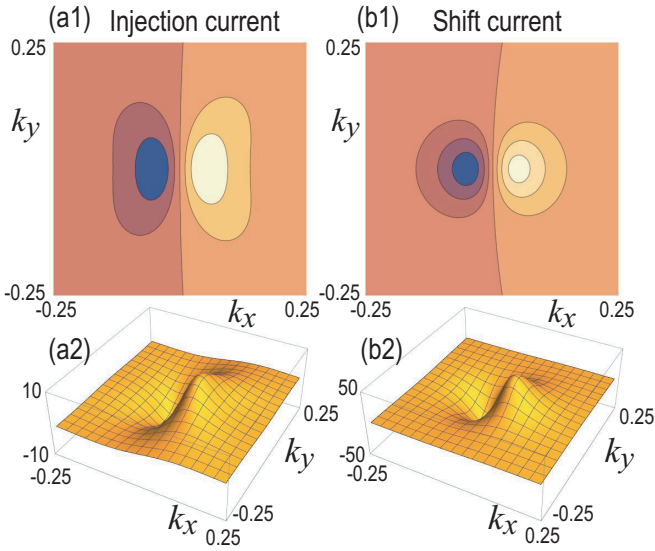


FIG. 3. (a1), (a2) $\Delta_{+-}^x |r_{-+}^x|^2$ in the k_x - k_y plane for the injection current. (b1), (b2) $\text{Re}(R_{+-}^{x,x} - R_{+-}^{x,y}) r_{-+}^y r_{+-}^x$ in the k_x - k_y plane for the shift current. (a1), (b1) Contour plot. (a2), (b2) Bird's eye's view. We have set $J = 0.1\epsilon_0/k_0^2$ and $B = 0.1\epsilon_0$.

in Eqs.(7) and Eq.(8) for a two-band system. By introducing the polar coordinate of the momentum, $k_x = k \cos \phi$, $k_y = k \sin \phi$, and by setting $\varepsilon(\mathbf{k}) \equiv \varepsilon(k, \phi)$, it is straightforward to derive the formula

$$\begin{aligned} \sigma_{\text{inject}}^{x;xx} &= -\tau \frac{2\pi e^3}{\hbar^2 W} \int \frac{k dk d\phi}{(2\pi)^2} (f_- - f_+) \Delta_{+-}^x r_{-+}^x r_{+-}^x \delta\left(\frac{2\varepsilon}{\hbar} - \omega\right) \\ &= -\tau \frac{2\pi e^3}{(2\pi)^2 \hbar^2 W} \int k \left. \frac{\Delta_{+-}^x |r_{-+}^x|^2}{2 |\partial_k \varepsilon| / \hbar} \right|_{k=k_\omega(\phi)} d\phi \end{aligned} \quad (11)$$

for the injection current (7), and

$$\begin{aligned} \sigma_{\text{shift}}^{x;xy} &= -\frac{\pi e^3}{\hbar^2 W} \int \frac{k dk d\phi}{(2\pi)^2} (f_- - f_+) (R_{+-}^{x,x} - R_{+-}^{x,y}) r_{-+}^y r_{+-}^x \\ &\quad \times \delta\left(\frac{2\varepsilon}{\hbar} - \omega\right) \\ &= -\frac{\pi e^3}{(2\pi)^2 \hbar^2 W} \int k \left. \frac{(R_{+-}^{x,x} - R_{+-}^{x,y}) r_{-+}^y r_{+-}^x}{2 |\partial_k \varepsilon| / \hbar} \right|_{k=k_\omega(\phi)} d\phi \end{aligned} \quad (12)$$

for the shift current (8), where W is the width of the sample given by $W^{-1} = (2\pi)^{-1} \int dk_z$, and $k_\omega(\phi)$ is given by solving $2\varepsilon(k_\omega(\phi), \phi) = \hbar\omega$.

It is notable that the injection current and the shift current do not depend on the effective mass M . This is because the Berry connection r_{mn}^a , the interband transition of the velocity Δ_{mn}^c and the shift vector $R_{mn}^{c,a}$ are solely determined by h_j with $j = x, y, z$.

We determine the critical frequency ω_c exactly in the case

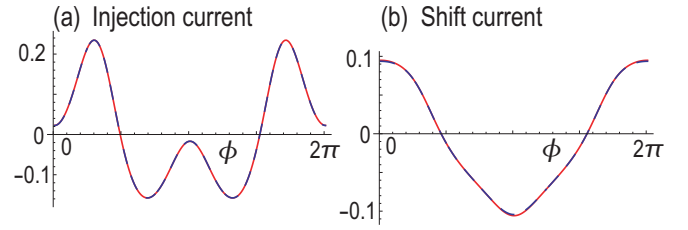


FIG. 4. (a) $\Delta_{+-}^x |r_{-+}^x|^2$ as a function of ϕ for the injection current. (b) $\text{Re}(R_{+-}^{x,x} - R_{+-}^{x,y}) r_{-+}^y r_{+-}^x$ as a function of ϕ for the shift current. The blue dashed curves are the numerical results without using the perturbation theory, while the red curves are the analytical results based on the perturbation theory. The agreement is remarkable. We have set $\hbar\omega = 0.4\epsilon_0$, $J = 0.1\epsilon_0/k_0^2$ and $B = 0.1\epsilon_0$.

of $J = 0$. The condition $\varepsilon_-(\mathbf{k}_c) \equiv \varepsilon_-(k_c, \phi_c) = 0$ gives

$$k_c = \sqrt{2} \sqrt{M^2 \lambda^2 + M \sqrt{M^2 \lambda^4 + B^2}}. \quad (13)$$

Then, the critical energy is obtained as

$$\hbar\omega_c = 2\varepsilon(k_c) = 2\sqrt{\lambda^2 k_c^2 + B^2}. \quad (14)$$

The effect of J to ω_c is found to be tiny comparing with the bulk band gap $2|B|$. We derive various formulas valid up to the first order in $J/(W\lambda)$ in what follows.

We show the energy spectrum $\varepsilon_\pm(\mathbf{k})$ along the k_x axis in Fig.2(a). It is asymmetric along the k_x direction for $J \neq 0$. It enables the emergence of the injection current and the shift current. The Fermi surface is shown as a red ellipse in Fig.2(b). Up to the first order in $J/(W\lambda)$, the energy of the Hamiltonian (9) is given by

$$\varepsilon(k, \phi) = \frac{\hbar^2 k^2}{2M} + \sqrt{\lambda^2 k^2 + B^2} + \frac{J k^3 (\cos \phi + \cos 3\phi)}{\sqrt{\lambda^2 k^2 + B^2}}. \quad (15)$$

To calculate Eqs.(11) and (12), it is necessary to solve $2\varepsilon(k_\omega(\phi), \phi) = \hbar\omega$. Solving it we obtain

$$k_\omega(\phi) = \frac{\sqrt{(\hbar\omega)^2 - 4B^2}}{2\lambda} - \frac{J \left((\hbar\omega)^2 - 4B^2 \right) (\cos \phi + \cos 3\phi)}{8\lambda^3}. \quad (16)$$

It is shown as a cyan ellipse in Fig.2(b). It well reproduces the numerical result without using the perturbation theory shown in red ellipse.

Injection current: We study the injection current by applying linearly polarized light. The integrand $\Delta_{+-}^x |r_{-+}^x|^2$ in Eq.(7) is shown in the k_x - k_y plane in Fig.3(a1) and (a2). The integration is done on the ellipse $k_\omega(\phi)$ given in Eq.(16), which is shown in Fig.4(a). The injection current Eq.(11) is obtained up to the first order in $J/(W\lambda)$ as

$$\sigma_{\text{inject}}^{x;xx} = -\tau \frac{e^3}{8\hbar^2 W\lambda} \frac{J}{\left(1 + 8 \left(\frac{B}{\hbar\omega}\right)^2 - 48 \left(\frac{B}{\hbar\omega}\right)^4\right)}. \quad (17)$$

When the applied energy ω is much larger than the band gap $\varepsilon_{\text{gap}} = 2|B|$, the injection current is independent of B and has

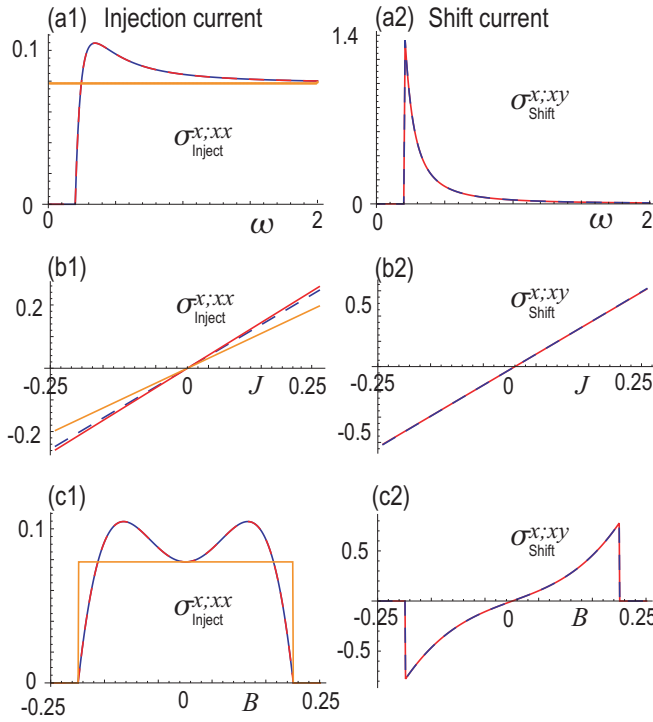


FIG. 5. (a1), (a2) Current as a function of $\hbar\omega/\varepsilon_0$. We have set $J = 0.1\varepsilon_0/k_0^2$ and $B = 0.1\varepsilon_0$. (b1), (b2) Current as a function of $\frac{J}{W\lambda}$. We have set $B = 0.1\varepsilon_0$ and $\hbar\omega = 0.4\varepsilon_0$. (c1), (c2) Current as a function of B/ε_0 . We have set $J = 0.1\varepsilon_0/k_0^2$ and $\hbar\omega = 0.4\varepsilon_0$. (a1), (b1), (c1) Injection current $\sigma_{\text{inject}}^{x;xx}$ in units of $-\tau \frac{e^3}{8\hbar^2} \frac{J}{W\lambda}$. (a2), (b2), (c2) The shift current $\sigma_{\text{shift}}^{x;xy}$ in units of $\frac{e^3}{4\hbar^2} \frac{J}{W\lambda}$. The blue dashed curves are the numerical results without using the perturbation theory, while the red curves are the analytical results based on the perturbation theory. The agreement is remarkable. Orange lines are the result for $B \ll \hbar\omega$ given in Eq.(18). The critical energy is $\hbar\omega_c \simeq 8\varepsilon_0$.

a simple form

$$\sigma_{\text{inject}}^{x;xx} = -\tau \frac{e^3}{8\hbar^2} \frac{J}{W\lambda}, \quad (18)$$

which is the illustration in Fig.1(c). The injection current is shown as a function of ω in Fig.5(a1), as a function of J in Fig.5(b1), and as a function of B in Fig.5(c1). The numerical result and the perturbation result well agree one to another. The injection current is almost independent of the applied frequency ω .

Similary, we have

$$\sigma_{\text{inject}}^{x;yy} = -\tau \frac{e^3}{8\hbar^2} \frac{J}{W\lambda} \left(1 - 2 \left(\frac{B}{\hbar\omega} \right)^2 + 4 \left(\frac{B}{\hbar\omega} \right)^4 \right), \quad (19)$$

and

$$\sigma_{\text{inject}}^{x;xy} = -\tau \frac{e^3}{8\hbar^2} \frac{iJ\pi}{\lambda} \frac{B}{\hbar\omega} \left(1 - 4 \left(\frac{B}{\hbar\omega} \right)^2 \right). \quad (20)$$

Then, the injection currents induced by the circularly polarized light (6) are given by

$$\sigma_{\text{inject}}^{x;\odot} = -\tau \frac{e^3}{8\hbar^2} \frac{J}{W\lambda} (2 + 2B) + o(B^3), \quad (21)$$

and

$$\sigma_{\text{inject}}^{x;\odot} = -\tau \frac{e^3}{8\hbar^2} \frac{J}{W\lambda} (2 - 2B) + o(B^3). \quad (22)$$

Shift current: Next, we study the shift current. The real part of $(R_{+-}^{x,x} - R_{-+}^{x,y}) r_{-+}^y + r_{+-}^x$ in Eq.(8) is shown in the k_x - k_y plane in Fig.3(b1) and (b2). The integration is done on the ellipse $k_\omega(\phi)$ given in Eq.(16), which is shown in Fig.4(b). The transverse conductivity $\sigma_{\text{shift}}^{x;xy}$ Eq.(12) is obtained up to the first order in $J/(W\lambda)$ as

$$\sigma_{\text{shift}}^{x;xy} = \frac{1}{\omega} \frac{e^3}{4\hbar^2} \frac{J}{W\lambda} \frac{B}{\hbar\omega} \left(1 + 4 \left(\frac{B}{\hbar\omega} \right)^2 \right), \quad (23)$$

which is the illustration in Fig.1(b). It vanishes for the gapless system with $B = 0$. The current is generated proportional to $1/\omega$. It is shown as a function of ω in Fig.5(a2), as a function of J in Fig.5(b2) and as a function of B in Fig.5(c2). It is induced by the linearly polarized light with $\phi = \pi/4$. On the other hand, the shift current is not generated by applying the circularly polarized light because the transverse conductivity $\sigma_{\text{shift}}^{x;xy}$ is real[5], where the imaginary part of the transverse conductivity is necessary[9].

On the other hand, explicit calculations show that the shift current is zero $\sigma_{\text{shift}}^{x;xx} = \sigma_{\text{shift}}^{x;yy} = 0$, when the linearly polarized light is applied. Hence, the shift current is not generated by applying the circularly polarized light,

$$\sigma_{\text{shift}}^{x;\odot} = \sigma_{\text{shift}}^{x;\odot} = 0. \quad (24)$$

Discussion: Bulk photovoltaic effects are useful for future solar cell technology because they produce the direct current from alternating electric field. Solar light has a continuous frequency spectrum. In the viewpoint of applications, the injection current has greater merits than the shift current. Indeed, all photons within a wide range of frequency contribute almost equally to the injection current. On the other hand, although the shift current is generated from all photons within the same range, the magnitude is proportional to $1/\omega$. Namely, the contribution from photons with high frequency ω is small. Furthermore, the injection current has a finite contribution even for $B = 0$. It means that B can be infinitesimally small because it is only necessary for making a finite gap so that the Berry connection is well defined. The geomagnetism may be enough for small B . On the other hand, the shift current is proportional to B , where it is necessary to introduce large B . It is done by attaching a ferromagnet to the sample. However, it degrades the transparency to inject a light into the sample. Finally, the injection current is proportional to the relaxation time τ . Then, the injection current is enhanced for a clean sample. On the other hand, the shift current is independent of τ , where the shift current cannot be enhanced even for a clean sample.

In this work we made the perturbation in the parameter $J/(W\lambda)$, whose validity we discuss. A typical value of the Rashba interaction is $\lambda = 0.33\text{eV}\text{\AA}$ at the Au(111) surface[60]. A typical value[61] of J is $J = 30\text{meV}\times a^2$ with the lattice constant a , where a is of the order of 10\AA . Hence, we have $J/(W\lambda) \sim a/W \ll 1$ and the perturbation is justified, where the width W is typically $W > 100a$.

We make a comment on the terminology in Ref.[21], where the injection current (7) is decomposed into the normal and magnetic injection currents, and a similar decomposition for the shift current (8). Here, only the normal ones emerge in the system with time-reversal symmetry, while both the normal and magnetic ones may emerge in the system without time-reversal symmetry. The present system (9) has no time-reversal symmetry. The injection current (17) induced by the linear polarized light is identical to the magnetic injection current[21, 45], while the injection currents (21) and (22) induced by circularly polarized light are checked to be the normal injection currents and there is no magnetic injection cur-

rent. On the other hand, the shift current induced by linearly polarized light (23) is the normal shift current and there is no shift current induced by the circularly polarized light.

The main result of this work is that the injection current is almost independent for $\varepsilon_{\text{gap}} < \hbar\omega < \hbar\omega_c$, which is derived based on a simple two-band model. This result may be modified in actual experiments due to two reasons[7]. First, the complex band structures of real materials cannot be accurately captured by this simple two-band model. Second, the effects of electron-hole interactions or many-body interactions may change the spectrum of the injection current. It would be interesting to make an experimental study of a system made of d -wave altermagnets with the Rashba interaction, where various energy can be harvested over a wide range of ω via the injection current.

The author is very much grateful to T. Morimoto and N. Nagaosa for helpful discussions on the subject. This work is supported by CREST, JST (Grants No. JPMJCR20T2) and Grants-in-Aid for Scientific Research from MEXT KAKENHI (Grant No. 23H00171).

-
- [1] V. I. Belinicher and B. I. Sturman, The photogalvanic effect in media lacking a center of symmetry, Sov. Phys. Usp. 23, 199 (1980).
- [2] W. Kraut and R. von Baltz, Anomalous bulk photo-voltaic effect in ferroelectrics: A quadratic response theory, Phys. Rev. B 19, 1548 (1979).
- [3] Ralph von Baltz and Wolfgang Kraut, Theory of the bulk photovoltaic effect in pure crystals, Phys. Rev. B 23, 5590 (1981)
- [4] C. Aversa and J. E. Sipe, Nonlinear Optical Susceptibilities of Semiconductors: Results with a Length-Gauge Analysis, Phys. Rev. B 52, 14636 (1995)
- [5] J. E. Sipe and A. I. Shkrebtii, Second-order optical response in semiconductors, Phys. Rev. B 61, 5337 (2000).
- [6] V. M. Fridkin, Bulk photovoltaic effect in noncentrosymmetric crystals, Crystallogr. Rep. 46, 654 (2001).
- [7] Fernando de Juan, Adolfo G. Grushin, Takahiro Morimoto, Joel E. Moore, Quantized circular photogalvanic effect in Weyl semimetals, Nature Communications 8, 15995 (2017).
- [8] F. de Juan, Y. Zhang, T. Morimoto, Y. Sun, J. E. Moore, and A.G. Grushin, Difference Frequency Generation in Topological Semimetals, Phys. Rev. Research 2, 012017 (2020).
- [9] Junyeong Ahn, Guang-Yu Guo, and Naoto Nagaosa, Low-Frequency Divergence and Quantum Geometry of the Bulk Photovoltaic Effect in Topological Semimetals, Phys. Rev. X 10, 041041 (2020).
- [10] Yiyang Jiang, Tobias Holder, and Binghai Yan, Revealing Quantum Geometry in Nonlinear Quantum Materials, arXiv:2503.04943.
- [11] Hikaru Watanabe and Youichi Yanase, Chiral Photocurrent in Parity-Violating Magnet and Enhanced Response in Topological Antiferromagnet, Phys. Rev. X, 11, 011001 (2021)
- [12] Shun Okumura, Takahiro Morimoto, Yasuyuki Kato, and Yukitoshi Motome, Quadratic optical responses in a chiral magnet, Phys. Rev. B 104, L180407 (2021)
- [13] Z. Dai and A. M. Rappe, Recent progress in the theory of bulk photovoltaic effect, Chemical Physics Reviews 4, 011303 (2023).
- [14] J. Ahn, G.-Y. Guo, N. Nagaosa, A. Vishwanath, Riemannian geometry of resonant optical responses, Nature Physics 18, 290 (2022)
- [15] S. M. Young and A. M. Rappe, First Principles Calculation of the Shift Current Photovoltaic Effect in Ferroelectrics, Phys. Rev. Lett. 109, 116601 (2012).
- [16] S. M. Young, F. Zheng, and A. M. Rappe, First-Principles Calculation of the Bulk Photovoltaic Effect in Bismuth Ferrite, Phys. Rev. Lett. 109, 236601 (2012).
- [17] T. Morimoto and N. Nagaosa, Topological nature of nonlinear optical effects in solids, Science Advances 2, e1501524 (2016)
- [18] Kun Woo Kim, Takahiro Morimoto, and Naoto Nagaosa, Shift charge and spin photocurrents in Dirac surface states of topological insulator, Phys. Rev. B, 95, 035134 (2017)
- [19] T. Barik and J. D. Sau, Nonequilibrium nature of nonlinear optical response: Application to the bulk photovoltaic effect, Phys. Rev. B 101, 045201 (2020).
- [20] Hiroki Yoshida and Shuichi Murakami, Diverging shift current responses in the gapless limit of two-dimensional systems, arXiv:2407.18565
- [21] Hua Wang and Xiaofeng Qian, Electrically and magnetically switchable nonlinear photocurrent in PT-symmetric magnetic topological quantum materials, npj Computational Materials 6, 199 (2020)
- [22] Lukas Braun, Gregor Mussler, Andrzej Hruban, Marcin Konczykowski, Thomas Schumann, Martin Wolf, Markus Munzenberg, Luca Perfetti and Tobias Kampfrath Ultrafast photocurrents at the surface of the three-dimensional topological insulator Bi 2 Se3, Nature Commun. 7, 13259 (2016)
- [23] M. Nakamura, S. Horiuchi, F. Kagawa, N. Ogawa, T. Kurumaji, Y. Tokura and M. Kawasaki, Shift current photovoltaic effect in a ferroelectric charge-transfer complex, Nature Communications 8, 281 (2017)
- [24] M. Sotome, M. Nakamura, J. Fujioka, M. Ogino, Y. Kaneko, T. Morimoto, Y. Zhang, M. Kawasaki, N. Nagaosa, Y. Tokura, N. Ogawa, Spectral dynamics of shift current in ferroelectric semiconductor SbSI, PNAS 116, 1929 (2019)
- [25] Gavin B. Osterhoudt, Laura K. Diebel, Mason J. Gray, Xu Yang, John Stanco, Xiangwei Huang, Bing Shen, Ni Ni, Philip

- J. W. Moll, Ying Ran and Kenneth S. Burch, Colossal mid-infrared bulk photovoltaic effect in a type-I Weyl semimetal Nature Materials 18, 471 (2019)
- [26] Hiroki Hatada, Masao Nakamura, Masato Sotome, Yoshio Kaneko, Naoki Ogawa, Takahiro Morimoto, Yoshinori Tokura, Masashi Kawasaki, Defect tolerant zero-bias topological photocurrent in a ferroelectric semiconductor, PNAS 117, 20411 (2020)
- [27] Libor Šmejkal, Jairo Sinova, and Tomas Jungwirth, Emerging Research Landscape of Altermagnetism, Phys. Rev. X 12, 040501 (2022).
- [28] L. Smejkal, J. Sinova, and T. Jungwirth, Beyond Conventional Ferromagnetism and Antiferromagnetism: A Phase with Non-relativistic Spin and Crystal Rotation Symmetry, Phys. Rev. X, 12, 031042 (2022).
- [29] L. Smejkal, A. H. MacDonald, J. Sinova, S. Nakatsuji and T. Jungwirth, Anomalous Hall antiferromagnets, Nat. Rev. Mater. 7, 482 (2022).
- [30] Makoto Naka, Satoru Hayami, Hiroaki Kusunose, Yuki Yanagi, Yukitoshi Motome and Hitoshi Seo, Spin current generation in organic antiferromagnets, Nat. Com. 10, 4305 (2019).
- [31] K.-H. Ahn, A. Hariki, K.-W. Lee, and J. Kunes, Antiferromagnetism in RuO_2 as d-wave Pomeranchuk instability, Phys. Rev. B 99, 184432 (2019).
- [32] Rafael Gonzalez-Hernandez, Libor Šmejkal, Karel Vborn, Yuta Yahagi, Jairo Sinova, Tomš Jungwirth, and Jakub Železn, Efficient electrical spin splitter based on nonrelativistic collinear antiferromagnetism, Phys. Rev. Lett., 126:127701, (2021).
- [33] M Naka, Y Motome, and H Seo, Perovskite as a spin current generator. Phys. Rev. B, 103, 125114, (2021).
- [34] Arnab Bose, Nathaniel J. Schreiber, Rakshit Jain, Ding-Fu Shao, Hari P. Nair, Jiaxin Sun, Xiyue S. Zhang, David A. Muller, Evgeny Y. Tsymbal, Darrell G. Schlom and Daniel C. Ralph, Tilted spin current generated by the collinear antiferromagnet ruthenium dioxide, Nature Electronics 5, 267 (2022).
- [35] Makoto Naka, Yukitoshi Motome and Hitoshi Seo, Altermagnetic Perovskites, npj Spintronics volume 3, 1 (2025)
- [36] S. Hayami, Y. Yanagi, and H. Kusunose, Momentum-Dependent Spin Splitting by Collinear Antiferromagnetic Ordering, J. Phys. Soc. Jpn. 88, 123702 (2019).
- [37] Rina Takagi, Ryosuke Hirakida, Yuki Settai, Rikuto Oiwa, Hirotaka Takagi, Aki Kitaori, Kensei Yamauchi, Hiroki Inoue, Jun-ichi Yamaura, Daisuke Nishio-Hamane, Shinichi Itoh, Seno Aji, Hiraku Saito, Taro Nakajima, Takuya Nomoto, Ryotaro Arita and Shinichiro Seki, Spontaneous Hall effect induced by collinear antiferromagnetic order at room temperature, Nature Materials (2024)
- [38] Yuan Fang, Jennifer Cano, and Sayed Ali Akbar Ghorashi, Quantum Geometry Induced Nonlinear Transport in Altermagnets, Phys. Rev. Lett. 133, 106701 (2024).
- [39] M. Ezawa, Intrinsic nonlinear conductivity induced by quantum geometry in altermagnets and measurement of the in-plane Neel vector, Phys. Rev. B 110, L241405 (2024)
- [40] M. Ezawa, Third-order and fifth-order nonlinear spin-current generation in g-wave and i-wave altermagnets and perfect spin-current diode based on f-wave magnets, arXiv:2411.16036
- [41] T. Holder, D. Kaplan, and B. Yan, Consequences of Time-Reversal-Symmetry Breaking in the Light-Matter Interaction: Berry Curvature, Quantum Metric, and Diabatic Motion, Phys. Rev. Research 2, 033100 (2020).
- [42] Y.G. Semenov, X. Li, and K. W. Kim, Tunable Photogalvanic Effect on Topological Insulator Surfaces via Proximity Interactions, Phys. Rev. B 86, 201401(R) (2012).
- [43] N. Ogawa, R. Yoshimi, K. Yasuda, A. Tsukazaki, M. Kawasaki, and Y. Tokura, Zero-Bias Photocurrent in Ferromagnetic Topological Insulator, Nat. Commun. 7, 12246 (2016).
- [44] C.-K. Chan, N. H. Lindner, G. Refael, and P. A. Lee, Photocurrents in Weyl Semimetals, Phys. Rev. B 95, 041104(R) (2017).
- [45] Y. Zhang, T. Holder, H. Ishizuka, F. de Juan, N. Nagaosa, C. Felser, and B. Yan, Switchable Magnetic Bulk Photovoltaic Effect in the Two-Dimensional Magnet CrI_3 , Nat. Commun. 10, 3783 (2019).
- [46] Z. Sun, Y. Yi, T. Song, G. Clark, B. Huang, Y. Shan, S. Wu, D. Huang, C. Gao, Z. Chen et al., Giant Nonreciprocal Second-Harmonic Generation from Antiferromagnetic Bilayer CrI_3 , Nature (London) 572, 497 (2019).
- [47] Junta Iguchi, Hikaru Watanabe, Yuta Murakami, Takuya Nomoto, Ryotaro Arita, Bulk photovoltaic effect in antiferromagnet: Role of collective spin dynamics, Phys. Rev. B 109, 064407 (2024)
- [48] Yu-Xuan Li and Cheng-Cheng Liu, Majorana corner modes and tunable patterns in an altermagnet heterostructure, Phys. Rev. B 108, 205410 (2023).
- [49] Sayed Ali Akbar Ghorashi, Taylor L. Hughes, Jennifer Cano, Altermagnetic Routes to Majorana Modes in Zero Net Magnetization, Phys. Rev. Lett. 133, 106601 (2024).
- [50] Di Zhu, Zheng-Yang Zhuang, Zhigang Wu, and Zhongbo Yan, Topological superconductivity in two-dimensional altermagnetic metals, Phys. Rev. B 108, 184505 (2023)
- [51] M. Ezawa. Detecting the Neel vector of altermagnets in heterostructures with a topological insulator and a crystalline valley-edge insulator, Physical Review B 109 (24), 245306 (2024).
- [52] Yichen Liu, Junxi Yu, and Cheng-Cheng Liu, Twisted Magnetic Van der Waals Bilayers: An Ideal Platform for Altermagnetism, Phys. Rev. Lett. 133, 206702 (2024)
- [53] K.-H. Ahn, A. Hariki, K.-W. Lee, and J. Kunes, Antiferromagnetism in RuO_2 as d-wave Pomeranchuk instability, Phys. Rev. B 99, 184432 (2019).
- [54] L.Smejkal, R. Gonzalez-Hernandez, T.Jungwirth, and J. Sinova, Crystal time-reversal symmetry breaking and spontaneous Hall effect in collinear antiferromagnets. Science Advances 6, eaaz8809 (2020).
- [55] Teresa Tschirner, Philipp Keler, Ruben Dario Gonzalez Beattancourt, Tommy Kotte, Dominik Kriegner, Bernd Buechner, Joseph Dufouleur, Martin Kamp, Vedran Jovic, Libor Šmejkal, Jairo Sinova, Ralph Claessen, Tomas Jungwirth, Simon Moser, Helena Reichlova, Louis Veyrat, Saturation of the anomalous Hall effect at high magnetic fields in altermagnetic RuO_2 , APL Mater. 11, 101103 (2023)
- [56] O. Fedchenko, J. Minar, A. Akashdeep, S.W. D'Souza, D. Vasilyev, O. Tkach, L. Odenbreit, Q.L. Nguyen, D. Kutnyakhov, N. Wind, L. Wenthaus, M. Scholz, K. Rossnagel, M. Hoesch, M. Aeschlimann, B. Stadtmueller, M. Klaeui, G. Schoenhense, G. Jakob, T. Jungwirth, L. Šmejkal, J. Sinova, H. J. Elmers, Observation of time-reversal symmetry breaking in the band structure of altermagnetic RuO_2 , Science Advances 10, 5 (2024).
- [57] Zihan Lin, Dong Chen, Wenlong Lu, Xin Liang, Shiyu Feng, Kohei Yamagami, Jacek Osiecki, Mats Leandersson, Balasubramanian Thiagarajan, Junwei Liu, Claudia Felser, Junzhang Ma, Observation of Giant Spin Splitting and d-wave Spin Texture in Room Temperature Altermagnet RuO_2 , arXiv:2402.04995.
- [58] Miina Leiviski Javier Rial, Anton Badura, Rafael Lopes Seeger, Ismaa Kounta, Sebastian Beckert, Dominik Kriegner, Isabelle Jourard, Eva Schmoranzerov Jairo Sinova, Olena Gomonay, Andy Thomas, Sebastian T. B. Goennenwein, Helena Reichlov Libor Šmejkal, Lisa Michez, Tom Jungwirth, Vincent Baltz,

- Anisotropy of the anomalous Hall effect in the altermagnet candidate Mn_5Si_3 films, Phys. Rev. B 109, 224430 (2024)
- [59] I. I. Mazin, K. Koepernik, M.D. Johannes, Rafael Gonzalez-Hernandez, Libor Šmejkal, Prediction of unconventional magnetism in doped FeSb_2 , Proceedings of the National Academy of Sciences 118, e2108924118 (2021)
- [60] S. LaShell, B.A. McDougall, and E. Jensen, Spin Splitting of an $\text{Au}(111)$ Surface State Band Observed with Angle Resolved Photoelectron Spectroscopy, Phys. Rev. Lett. 77, 3419 (1996).
- [61] Yu-Xuan Li, Yichen Liu, and Cheng-Cheng Li, Creation and Manipulation of Higher-Order Topological States by Altermagnets, Phys. Rev. B 109, L201109 (2024)